2166–2178 *Nucleic Acids Research, 2017, Vol. 45, No. 4* *Published online 9 December 2016*
doi: 10.1093/nar/gkw1238

The AibR-isovaleryl coenzyme A regulator and its DNA binding site – a model for the regulation of alternative *de novo* isovaleryl coenzyme A biosynthesis in *Myxococcus xanthus*

Tobias Bock[1], Carsten Volz[2], Vanessa Hering[1], Andrea Scrima[3], Rolf Müller[2,*] and Wulf Blankenfeldt[1,4,*]

[1]Structure and Function of Proteins, Helmholtz Centre for Infection Research, Inhoffenstr. 7, 38124 Braunschweig, Germany, [2]Department of Microbial Natural Products, Helmholtz Institute for Pharmaceutical Research Saarland, Helmholtz Centre for Infection Research, Saarland University, 66123 Saarbrücken, Germany, [3]Structural Biology of Autophagy, Helmholtz Centre for Infection Research, Inhoffenstr. 7, 38124 Braunschweig, Germany and [4]Institute for Biochemistry, Biotechnology and Bioinformatics, Technische Universität Braunschweig, Spielmannstr. 7, 38106 Braunschweig, Germany

Received May 31, 2016; Revised November 25, 2016; Editorial Decision November 28, 2016; Accepted November 29, 2016

ABSTRACT

Isovaleryl coenzyme A (IV-CoA) is an important building block of iso-fatty acids. In myxobacteria, IV-CoA is essential for the formation of signaling molecules involved in fruiting body formation. Leucine degradation is the common source of IV-CoA, but a second, *de novo* biosynthetic route to IV-CoA termed AIB (alternative IV-CoA biosynthesis) was recently discovered in *M. xanthus*. The *AIB*-operon contains the TetR-like transcriptional regulator AibR, which we characterize in this study. We demonstrate that IV-CoA binds AibR with micromolar affinity and show by gelshift experiments that AibR interacts with the promoter region of the *AIB*-operon once IV-CoA is present. We identify an 18-bp near-perfect palindromic repeat as containing the AibR operator and provide evidence that AibR also controls an additional genomic locus coding for a putative acetyl–CoA acetyltransferase. To elucidate atomic details, we determined crystal structures of AibR in the apo, the IV-CoA- and the IV-CoA-DNA-bound state to 1.7 Å, 2.35 Å and 2.92 Å, respectively. IV-CoA induces partial unfolding of an α-helix, which allows sequence-specific interactions between AibR and its operator. This study provides insights into AibR-mediated regulation and shows that AibR functions in an unusual TetR-like manner by blocking transcription not in the ligand-free but in the effector-bound state.

INTRODUCTION

Myxobacteria are swarming soil-populating bacteria that exhibit a complex developmental cycle to survive critical environmental changes (1,2). To promote this life style, they have an enormous metabolic potential, reflected for instance in the use of unusual biochemistry in biosynthesis. One example is the production of isovaleryl coenzyme A (IV-CoA). This molecule is an important substance for myxobacteria as it is used as a building block for certain fatty acids and secondary metabolites needed during development (3–7). These iso-odd fatty acids maintain the membrane fluidity and serve as signaling molecules during differentiation (8,9). Typically, IV-CoA is generated by the branched-chain α-keto acid dehydrogenase complex (Bkd) acting during leucine degradation. However, Bode *et al.* (10) showed that the model myxobacterium, *Myxococcus xanthus*, harbors an additional route to produce IV-CoA from acetyl-CoA under leucine-limited conditions. By using global gene expression analysis and biochemical investigation the genes involved in this additional pathway, assigned as alternative IV-CoA biosynthesis (AIB), have been determined (10,11). These genes are clustered in the *AIB*-operon, which appeared to be highly active under leucine-limiting conditions. It contains five open reading frames coding for two subunits of a novel type of decarboxylase (AibA/AibB) (11), a dehydrogenase (AibC), a 3-hydroxyl-3-methylglutaryl coenzmye A synthase (MvaS) (12) and a regulatory protein (AibR). Furthermore, a gene coding for a 3-hydroxy-3-methylglutaryl coenzyme A dehydratase (LiuC), located in another operon, was shown to be involved in the pathway as well. MvaS converts acetyl coen-

*To whom correspondence should be addressed. Tel: +49 531 6181 7000; Fax: +49 531 6181 7099; Email: wulf.blankenfeldt@helmholtz-hzi.de
Correspondence may also be addressed to Rolf Müller. Tel: +681 98806 3000; Fax: +681 98806 3009; Email: rolf.mueller@helmholtz-hzi.de

zyme A (Ac-CoA) and acetoacetyl coenzyme A (AcAc-CoA) to 3-hydroxy-3-methylglutaryl coenzyme A (HMG-CoA), which is then dehydrated by LiuC. The resulting 3-methylglutaconyl coenzyme A (MG-CoA) is decarboxylated by AibA/AibB and further reduced by AibC, leading to the final product IV-CoA (Figure 1) (11).

The first gene of the *AIB*-operon, *aibR*, encodes a transcriptional regulator that has been shown to be involved in negative transcriptional regulation of the entire operon (13). Based on sequence analysis, AibR belongs to the TetR family repressors (TFR), which are named after the famous member involved in regulating tetracycline resistance genes (14). TetR-like proteins consist of nine α-helices arranged in a N-terminal helix turn helix motif also known as DNA binding domain (DBD) and a C-terminal ligand binding or sensory domain (LBD). This LBD interacts with the respective effector molecule and transmits the signal to the DBD (15,16). The active form of TFRs is a dimer that binds to a palindromic promoter sequence via contacts of helix α3 and α1 with the major groove of the DNA, respectively (17). Typically, the regulator shows higher affinity toward DNA in the ligand free-state, resulting in repression of transcription. After ligand binding, a conformational change and a reorientation of helix α3 results in a decrease of DNA affinity and gene transcription. This has been shown for example for FabR and FadR from *Escherichia coli*, which regulate fatty acid biosynthesis or degradation (18,19), and in other TFRs involved in the regulation of different cellular processes like antibiotic resistance, metabolism or cell–cell signaling (17). In addition to the typical role as repressor, TFRs also appear as activators as shown for FasR from *Streptomyces coelicolor* (20) or *Corynebacterium glutamicum*, both showing an increase in DNA affinity after ligand binding (21).

The regulation of IV-CoA biosynthesis is very important for myxobacteria, since this molecule is crucial for several metabolic processes and cellular functions. This importance is also reflected in the fact that myxobacteria have evolved the unique *AIB*-mediated route to produce this molecule (10). However, the regulation of IV-CoA production by AibR has not been investigated until now. Because of the great variety of TFR ligands and the sequence diversity of the ligand binding domains of these proteins, it is generally difficult to predict the identity of their cognate effector molecule(s), even if their target genes are known (17).

Here, we describe the identification of IV-CoA as the effector molecule controlling DNA-binding of AibR and we identify an 18-bp near-perfect inverted DNA-repeat as the operator sequence. Further, we provide detailed structural insights into effector and DNA binding by determination of crystal structures of AibR in the ligand-free and in the IV-CoA bound state as well as in complex with IV-CoA and a 16-bp segment of the operator sequence. With these, we are able to track the signal transduction between the LBD and the DBD upon IV-CoA binding and show in binding experiments that AibR interacts with the operator sequence only in the Iigand-bound state. Further, we identify one additional locus in the genome of *Myxococcus xanthus* that is predicted to interact with AibR and we propose a mode of transcriptional regulation of the myxobacterial AIB.

MATERIALS AND METHODS

Cloning and expression

Expression plasmid pET28a-*aibR* encoding for AibR N-terminally tagged with a thrombin-cleavable His_6-tag was freshly transformed into chemically competent *E. coli* BL21(DE3) cells and subsequently used for preculture inoculation supplemented with 50 mg l^{-1} kanamycin. The large-scale production was carried out in terrific broth including the same antibiotic. The cells were incubated at 37°C (310 K) and 120 rpm until the optical density at 600 nm reached 0.8. At this step, the temperature was reduced to 20°C (293 K), heterologous gene expression was induced with 500 μM isopropyl-ß-D-thiogalactopyranoside for another 20 h. Cells were harvested by centrifugation at 5000 *g* for 10 min and flash frozen in liquid nitrogen until needed.

L-seleno-methionine labeled AibR was produced in minimal media (M9) as described elsewhere (22). The LB pre-culture was centrifuged and washed with M9 minimal media before inoculation of a larger culture in M9 media with 50 mg l^{-1} kanamycin at 37°C (310 K) and 120 rpm. An amino acid cocktail comprising 100 mg l^{-1} lysine, 100 mg l^{-1} phenylalanine, 100 mg l^{-1} threonine, 50 mg l^{-1} isoleucine, 50 mg l^{-1} leucine and 50 mg l^{-1} valine was added to the cell suspension to suppress methionine biosynthesis when the optical density at 600 nm reached 0.5. After an additional incubation of 15 min, 60 mg l^{-1} L-seleno-methionine and 500 μM isopropyl-ß-D-thiogalactopyranoside were added to the cells and the culture was further incubated at 20°C (293 K) for 20 h.

Purification

Cells were diluted with buffer A (50 mM TRIS pH 7.8; 300 mM NaCl; 20 mM imidazole) and subsequently lysed using an 'EmulsiFlex-C3 homogenizer' (AVESTIN®). To remove insoluble parts the cell suspension was centrifuged at 30 000 *g* for 45 min at 4°C (277 K). The cleared supernatant was applied onto a HiTrap chelating column (GE Healthcare Life Science) loaded with 100 mM nickel sulfate and then equilibrated in buffer A. The column was washed with buffer A until the absorption at 280 nm reached the baseline again. Bound proteins were eluted with a three-step gradient, ranging from 10% to 20% and 60% buffer B (buffer A containing 500 mM imidazole). To remove the affinity tag, thrombin protease cleavage was carried out in a 1:20 molar ratio (protease to protein) over night at 4°C (277 K) during dialysis against buffer C (50 mM TRIS pH 7.0; 50 mM NaCl). Anion exchange chromatography using a HitrapQ column (GE Healthcare Life Science) was used to separate AibR from the residual His_6-tag and thrombin protease. Elution was performed with a linear gradient ranging from 0 to 1 M NaCl (Buffer D: 50 mM TRIS pH 7.0; 1 M NaCl). Fractions containing the recombinant protein were collected, concentrated and applied to an S200 16/60 size exclusion column (GE Healthcare Life Science) equilibrated with buffer E (50 mM TRIS pH 7.5; 100 mM NaCl). Fractions containing pure protein were collected, concentrated to 20 mg ml^{-1} and flash frozen. The L-seleno-methionine labeled protein was treated in the same way as described for the wild-type protein.

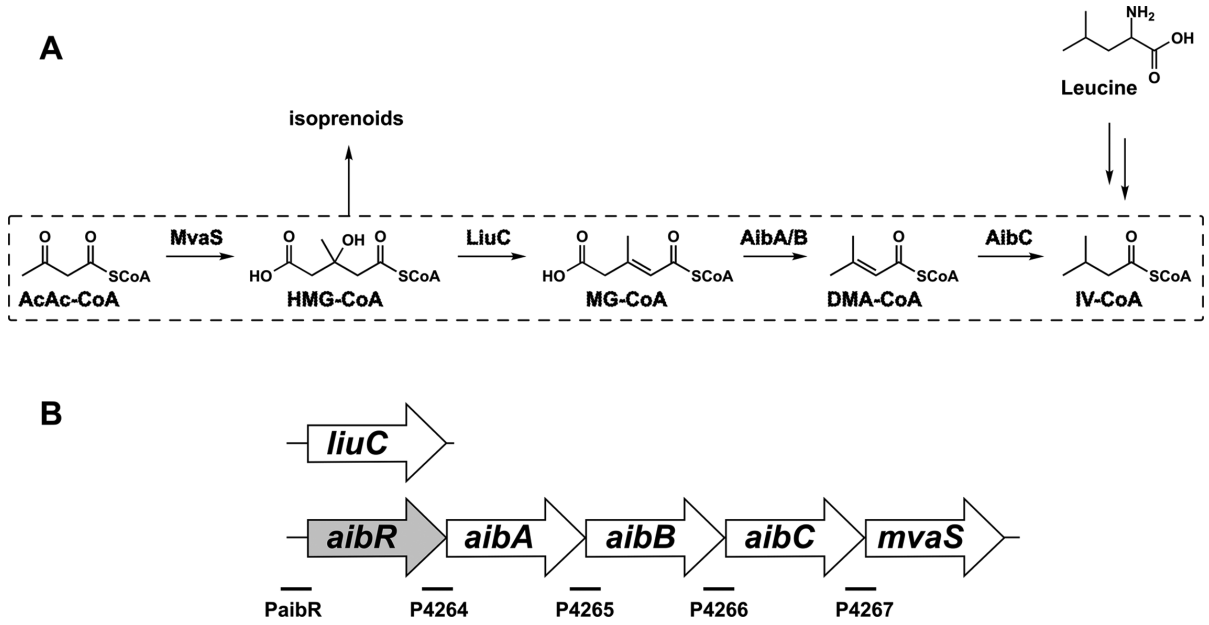

Figure 1. Alternative isovaleryl coenzyme A biosynthesis (AIB) in (**A**) *Myxococcus xanthus* and organization of the (**B**) *AIB*-operon. *aibR* is highlighted in grey. The alternative isovaleryl coenzyme A pathway is marked by the dotted line. AcAc-CoA: acetoacetyl CoA, HMG-CoA: 3-hydroxy-3-methylglutaryl CoA; MG-CoA: 3-methylglutaconyl CoA, DMA-CoA: 3,3-dimethylacrylyl CoA; IV-CoA: isovaleryl CoA. Modified according to Liu *et al* (11). Black lines in (B) indicate the position and names of DNA segments tested for AibR binding.

Microscale thermophoresis

To determine the binding affinity between AibR and IV-CoA or other coenzyme A derivatives, microscale thermophoresis (MST) was used (23). For this, AibR was labeled with Cy^{TM}5 Mono NHS Ester (Amersham^{TM}) according to the vendor's manual. To determine K_D-values for IV-CoA and 3,3-dimethylacrylyl coenzyme A, a fixed final concentration of 200 nM AibR-Cy^{TM}5 was titrated with serial 1:1 dilutions of both ligands in labeling buffer (50 mM HEPES pH 7.5, 100 mM NaCl, 0.5 mg ml^{-1} bovine serum albumin), while 100 nM labeled AibR was used for the non-binding molecules Ac-CoA, acetoacetyl coenzyme A, HMG-CoA, CoA and isovaleric acid (IVA).

The determination of the K_D for the AibR/IV-CoA complex and the operator sequence was performed similarly with 100 nM of a Cy^{TM}5-labeled DNA fragment (5′-Cy^{TM}-GCT ACC TAC CGG TCG GTA GGT). To generate the respective DNA double strand, oligonucleotides Cy5_for (5′-Cy^{TM}-GCT ACC TAC CGG TCG GTA GGT) and Cy5_rev (5′-ACC TAC CGA CCG GTA GGT AGC) were mixed at equal concentrations, incubated for 10 min at 95°C (368 K) and cooled to room temperature overnight. The resulting DNA fragment was titrated with a serial 1:1 dilution of AibR/IV-CoA complex.

The experiments were performed using a NanoTemper Monolith™ NT.115 instrument with standard (for non-binding molecules) or premium coated capillaries (for binding ligands) at 25°C (293 K), 10% LED power and 40% MST power. For K_D determinination, experiments were executed in triplicates. The response value was averaged and plotted against the concentration of the ligands. K_D values were extracted by fitting to the quadratic equation shown below (Equation (1)), using the vendor's software (K_D fit in MO.Affinity Analysis software, NanoTemper).

$$F(C_T) = F_A + \frac{F_{AT}-F_A}{2C_A}\left(C_T + C_A + K_D - \sqrt{(C_T + C_A + K_D)^2 - 4C_T C_A}\right) \quad (1)$$

Here, F_A represents the response value of unbound labeled molecules, F_{AT} the response value of the complex of labeled and the unlabeled ligand molecules, C_A the concentration of labeled molecule and C_T the concentration of the unlabeled ligand molecule.

For the titration of AibR with IV-CoA, the highest ligand concentrations reproducibly led to a decrease of the MST response. These values were therefore not included in the K_D determination (Figure 2A).

Electrophoretic mobility shift assay

Fluorescent labeling of DNA fragments and electrophoretic mobility shift assays (EMSA) were performed as described before with modifications (24). In brief, the modifications were as follows: poly-dIdC (Poly(deoxyinosinic-deoxycytidylic acid sodium salt; Sigma-Aldrich) was used instead of salmon sperm DNA as competitor DNA at a final concentration of 25 ng μl^{-1}. A total of 0.8 pM of the labeled DNA fragments were used in each experiment. Purified AibR was added in a 10- to 1000-fold molar excess to the reactions (0.4–40 μM). All reactions were pipetted on ice prior to loading on the gels. EMSA assays were performed at 4°C (277 K) at 3.5 V cm^{-1} for 45 min. Supplementary Table S3 lists specific primers used for amplification of putative promoter regions and primers used for the construction of oligo-based EMSA-fragments.

For the determination of the K_D of the AibR/IV-CoA complex and the operator sequence in EMSA assays, a 40-

bp Cy™5-labeled dsDNA-fragment (aibR-Cy5) was generated as described for the MST measurements using the oligonucleotides aibR-wtF and 5′-Cy™-aibR-wtR. A total of 0.8 pM of the DNA-fragment was titrated with a serial 1:1 dilution of AibR/IV-CoA complex ranging from 10 nM to 5.12 μM. The experiment was performed in triplicates. Fluorescence of unbound DNA and DNA bound to the AibR/IV-CoA complex was recorded by scanning the gel with a Typhoon™ 9410 gel imager (GE Healthcare) using the excitation laser at 633 nm and an emission filter of 670 nm. The fluorescent signal in each DNA band was quantitated using the ImageJ software (25). Signals from blank regions of the EMSA gel were subtracted from the fluorescence values measured from DNA bands. The portion of DNA bound to the AibR/IV-CoA complex was determined using these background-subtracted values in the quotient bound DNA/(unbound DNA + bound DNA). The calculated amounts of bound DNA were subsequently plotted against the concentration of the AibR/IV-CoA complex. The resulting data were fit in a non-linear regression based on the Equation (2) in Excel (Microsoft) using the Solver add-in (26,27).

$$bound\ DNA = B_{\max} * \frac{[AibR/IVCoA]^2}{[AibR/IVCoA]^2 + K_D^2} \quad (2)$$

Here, B_{max} is the amount of DNA where a maximum of DNA was bound and a plateau was reached.

Crystallization, data collection and refinement

Initial crystallization conditions were identified at room temperature using the vapor diffusion method in a 96 well format. Screening was performed by mixing 0.2 μl AibR (20 mg ml^{-1}) and 0.2 μl reservoir solution using a HoneyBee dispensing robot (Zinsser Analytic, Frankfurt am Main, Germany). The drops were equilibrated against 70 μl reservoir solution. High-quality diffracting crystals were obtained after optimization by mixing 0.2 μl reservoir consisting of 0.1 M TRIS pH 7.4, 0.2 M ammonium acetate and 20% (w/v) PEG 3350 and 0.2 μl protein solution at 20 mg ml^{-1}. Reservoir supplemented with 10% (w/v) glycerol was used as cryo-protectant. L-seleno-methionine labeled AibR crystals were obtained from initial screening against reservoir containing 0.1 M TRIS pH 8.5, 0.2 M trimethylamine N-oxide and 20% polyethylene glycol monoethyl ether 2000. Crystals were cryo-protected with 10% (w/v) glycerol as well. Crystals of the AibR/IV-CoA complex were obtained by using the random microseeding approach (28). For this, 20 mg ml^{-1} AibR were mixed with 1 mM IV-CoA, incubated for 30 min at 4°C (277 K) and 0.2 μl mixed with 0.05 μl seeding solution and 0.15 μl reservoir solution using an OryxNano dispending robot (Douglas Instruments, Hungerford, UK). To produce the seeding solution, apo AibR crystals were crushed and diluted in 50 μl reservoir solution containing 0.1 M HEPES pH 7.6, 0.2 M ammonium acetate and 23% (w/v) PEG3350. Crystals of the complex appeared after 20 days in a condition comprising 0.1 M sodium acetate pH 4.6, 2 M sodium chloride and were used for diffraction data collection without cryo-protection. The complex of AibR, IV-CoA and a 16-bp DNA fragment was obtained by incubation of 20 mg ml^{-1} AibR, 1 mM IV-CoA and 470 μM DNA for 1 h at room temperature and mixing with reservoir comprising 35% 2-ethoxyethanol, 0.1 M imidazole pH 7.8 and 0.05 M calcium acetate at 4°C (277 K). The 16-bp DNA double strand was reconstituted by the incubation of a primer (5′-CCTACCGATCGGTAGG) dissolved in water at a concentration of 10 mM at 95°C (368 K) for 10 min and then cooled to room temperature overnight.

Diffraction data were collected at −173°C (100 K) on beamline X06DA-PXIII at Swiss Light Source (Paul Scherrer Institute, Villingen, Switzerland), on beamline ID 23.1 at European Synchrotron Radiation Facility (Grenoble, France) and on beamline BL14.1 operated by the Helmholtz–Zentrum Berlin at the BESSY II electron storage ring (Berlin–Adlershof, Germany (29)), indexed and integrated with XDS (30) or XDSAPP (31) and scaled with AIMLESS from the CCP4 package (32). Single anomalous diffraction data of an L-seleno-methionine labeled AibR crystal were collected at a wavelength of 0.97795 Å, data of the wild-type crystals at 1.0003 Å, for the IV-CoA complex at 0.97625 Å and for the DNA complex at 0.91841 Å. For the Se-single anomalous diffraction data, the hkl2map package was used to extract the anomalous signal, to locate the anomalous scatterers, for density modification and automated model building (33). In order to solve the wild-type, the IV-CoA and the DNA complex structures, the resulting model was used for rigid body refinement and molecular replacement in PHENIX, respectively (34). The structures were refined using alternating steps of manual adjustment in Coot (35) and maximum likelihood refinement with the TLS-option (translation-libration-screw refinement, (36)) in PHENIX (34). Restraints for IV-CoA were generated by using eLBOW in PHENIX (37). For the AibR/IV-CoA/DNA complex, two DNA double strands were modeled with 50% occupancy and subjected to occupancy refinement in PHENIX as well. Molprobity (38) was used for final structure validation. An overview of all data-collection, refinement statistics and corresponding PDB codes is provided in Supporting Table S1 and S2.

RESULTS

AibR specifically binds IV-CoA and the putative promotor region PaibR

To gain insight into the regulation of AIB by AibR, we aimed to identify DNA segments which are recognized and specifically bound by AibR. For this, it was first necessary to identify the molecule(s) that potentially modulate the activity of AibR. It has previously been shown that the transcription of *mvaS*, a gene belonging to the *AIB*-operon (Figure 1), is downregulated by the addition of isovalerate (3), which suggests that AibR inhibits the transcription of AIB-enzymes after binding isovalerate, a precursor of isovalerate or an activated form of isovalerate.

After cellular uptake, isovalerate is required to be transformed to IV-CoA by an unknown coenzyme A transferase. This suggests that coenzyme A derivatives produced during AIB bind to and control inhibitory activity of AibR, which we investigated with MST experiments. Of the tested molecules, only IV-CoA and 3,3-dimethylacrylyl coenzyme

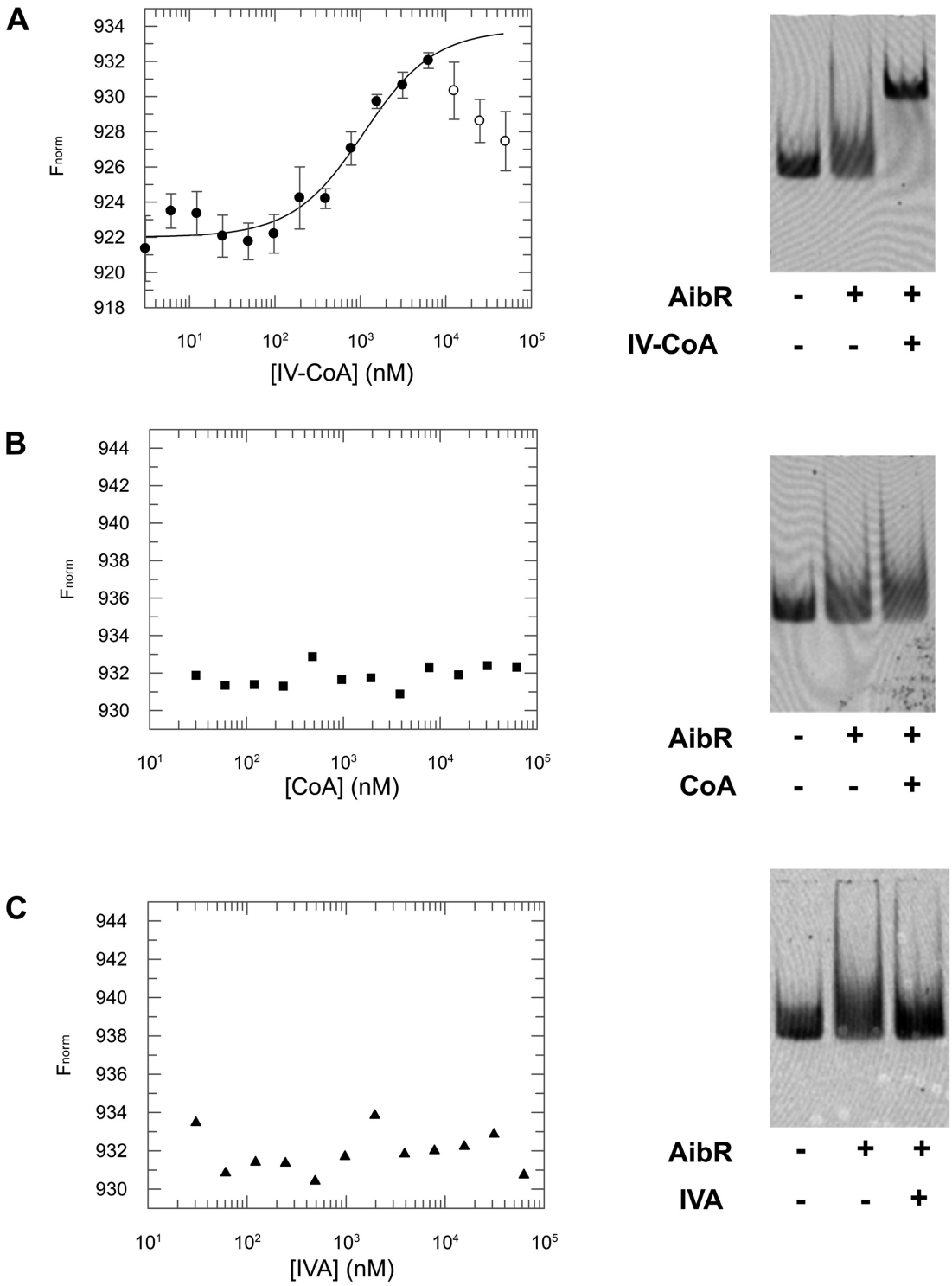

Figure 2. Identification of isovaleryl coenzyme A (IV-CoA) as effector molecule of AibR. **(A)** Microscale thermophoresis (MST) measurements reveal that IV-CoA binds AibR with a K_D of 0.99 μM ± 0.35 μM (left), enabling binding to PaibR in electrophoretic mobility shift assays (EMSA) analysis (right). **(B)** CoA and **(C)** IVA show no interaction with AibR. For details, refer to the Materials and Methods section.

A showed binding with K_Ds of 0.99 ± 0.35 μM and 5.8 ± 1.51 μM, respectively (Figure 2A and Supplementary Figure S1, S2A–C). In order to demonstrate that IV-CoA and not CoA or IVA binds AibR, we also measured interaction with these molecules. Neither CoA nor IVA bound, demonstrating the specificity of AibR for IV-CoA (Figure 2B and 2C).

Since transcriptional start sites of the *AIB*-operon are not known, we used amplified HEX-labeled DNA fragments of the *M. xanthus* DK1622 genome spanning upstream intergenic- and downstream regions of the annotated start codons of genes *aibR*, *aibA*, *aibB*, *aibC* and *mvaS* (mxan_4263 to mxan_4267) in initial EMSA assays with AibR. The DNA fragments were assigned PaibR, P4264, P4265, P4266 and P4267 (= putative promoter regions of the respective mxan-genes; Figure 1). In the absence of AIB-pathway intermediates, no binding of AibR to these DNA fragments was observed even in presence of a 1000-fold molar excess of the regulator protein (Supplementary Figure S3A). In a second series of EMSA assays, PaibR was incubated with AibR in presence of various ligands (Supplementary Figure S2D). Here, we indeed observed binding of AibR in the presence of IV-CoA as indicated by a clear shift in the gel retardation assay (Figure 2A). This shift was not observed with any of the other DNA fragments mentioned above (Supplementary Figure S3B), corroborating the hypothesis that AibR interacts with a specific DNA sequence in the putative promoter region PaibR, but only in the IV-CoA bound state.

Identification of the DNA binding site in the PaibR region and the first insight into the AibR regulon

In order to further narrow down the DNA binding site within the putative promoter PaibR, we divided the initial 310-bp PaibR DNA fragment into 12 regions of 40 bp length, each sharing a 20 bp overlap to their two neighboring regions (Supplementary Figure S4A). The respective DNA fragments were used in EMSA assays as Cy5-labeled DNA fragments aibR1 to aibR12 as described in the Materials and Methods section. In the presence of IV-CoA, we observed binding of AibR to DNA fragment aibR8 (Supplementary Figure S4A). Computational analysis revealed that this fragment contains the 18-nt near-perfect inverted repeat ACCTACCG-2N-CGGTAGGT with a spacer of two nucleotides (2N). We hypothesized this repeat to be the locus of AibR binding and corroborated this in subsequent EMSA analysis using mutated variants (two to five mutated positions per DNA fragment) in binding assays (Supplementary Figure S4B). Mutations reduced the binding affinity of AibR significantly as indicated by a reduced ability to form a complex with DNA. A final series of EMSA assays using variants mutated in every single position of the 18-nt inverted repeat (DNA fragments 3aibR1 to 3aibR18, Supplementary Table S3) revealed the influence of each nucleotide in binding to the AibR/IV-CoA complex (Figure 3A). Thirteen residues were found to be of importance for binding to AibR/IV-CoA by exhibiting either major or minor effects upon mutation. Major effects were observed after mutation of residues A5 or G8 (resulting in unstable, smeary complex formation), after mutation of T10 (decreased shift) and after mutation of G12 (completely abolished complex formation). Mutations of nine additional residues led to a decreased affinity as the shift was not quantitative when compared to the wild-type fragment.

The affinity of the AibR/IV-CoA complex for this operator sequence was determined with MST and EMSA analyses. Whereas MST with a Cy5-labeled 21-bp DNA molecule bound with relatively low affinity (K_D = 2.3 μM ± 0.85 μM, Supplementary Figure S1), EMSA assays using a 40-bp segment revealed approximately 10-fold tighter binding at K_D = 233 nM ± 20 nM (Figure 3B and Supplementary Figure S5A). A similar value was obtained with a fragment of approximately 190 bp. Although these results may be difficult to compare, these observations indicate that the affinity of AibR/IV-CoA toward longer DNA molecules is higher than to minimized fragments around the operator sequence.

A first search for additional copies of the AibR recognition sequence in the *Myxococcus xanthus* DK1622 genome revealed two additional loci in intergenic regions that have similar palindromic sequences and contain the important bases at positions 5, 8, 10 and 12, suggesting that the respective downstream genes may be controlled by AibR (see Supplementary Table S4). Noteworthy, one of these genes (mxan_3791) encodes for a putative acetyl-CoA acetyltransferase that most likely catalyzes the formation of acetoacetyl-CoA, one of the substrates of MvaS in AIB (Figure 1). Specific binding of AibR to the putative promoter region of mxan_3791 could indeed be demonstrated by EMSA analysis using DNA fragment P3791 (Figure 3C and Supplementary Figure S5B).

Taken together, these experiments reveal that AibR requires IV-CoA to interact with an 18-nt near-perfect inverted repeat in the 5′-region of the *AIB*-operon, of which most of the nucleotides 1–17 contribute to AibR binding. This sequence motif is also found in at least one further locus of the *Myxococcus xanthus* genome, providing first indications that the AibR regulon extends beyond the *AIB*-operon itself.

Structural insights into IV-CoA binding and specificity

To address atomic details of IV-CoA binding, we determined the crystal structure of AibR without and in complex with IV-CoA to 1.7 Å and 2.35 Å resolution, respectively. The ligand-free form crystallized in space group $P2_1$ and the complex in $P6_1$ with two chains in the asymmetric unit. According to the large interaction surface of 2440 $Å^2$ (16 900 $Å^2$ total surface area), AibR is a dimer, consistent with other TFRs and the apparent molecular weight observed in size exclusion chromatography. The interaction of both monomers is mainly hydrophobic and mediated by residues from helix α8 and α9. The AibR monomer possesses the typical TFR architecture characterized by nine α-helices, arranged in an N-terminal DNA-binding domain (α1–α3) connected via helix α4 with the larger C-terminal ligand-binding domain (α4–α9). The electrostatic surface potential of the DNA binding domain is predominantly positive, a feature important for the interaction with the phosphate groups of the DNA backbone (Supplementary Figure S6).

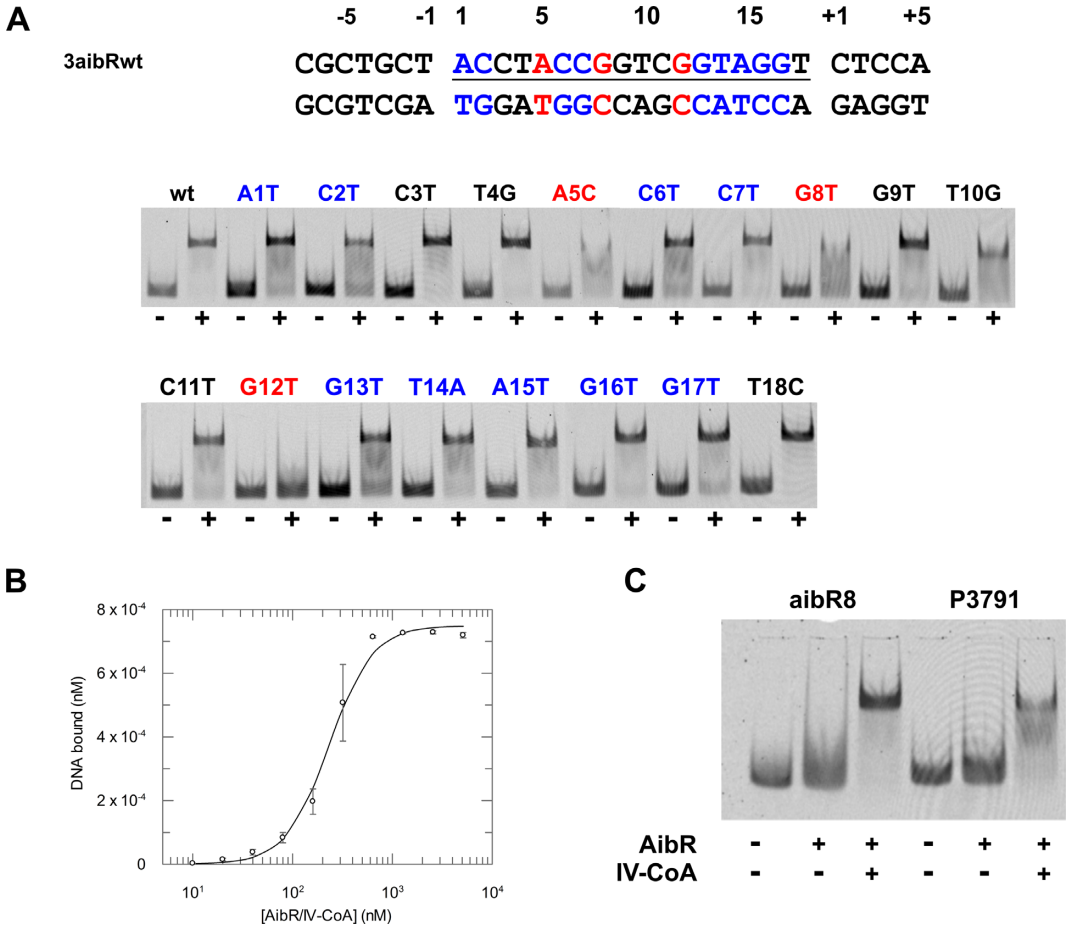

Figure 3. Binding of the AibR/IV-CoA complex to dsDNA in EMSAs. (**A**) Effect of single nucleotide mutations within the operator sequence. The sequence of DNA fragment 3aibRwt is shown at the top, the 18 nucleotides of the near-perfect inverted repeat (1-18) have been underlined. Red and blue indicate a strong and medium effect on the affinity toward AibR/IV-CoA. (**B**) Determination of the binding affinity of the AibR/IV-CoA complex and the operator sequence. Plot of bound labeled DNA versus the concentration of AibR/IV-CoA. Error bars were calculated from three independent assays. The calculated K_D based on the curve-fit is 233 nM ± 20 nM ($R^2 = 0.983$). (**C**) Identification of an additional locus putatively regulated by AibR. EMSA assay using Cy5-labeled DNA fragments aibR8 and P3791 (left). For details, refer to the Materials and Methods section.

The AibR dimer contains two IV-CoA binding sites that are independent of each other and span over both monomers (Figure 4A). These ligand binding sites can be divided into a solvent-exposed charged site interacting with the adenine moiety and a buried and hydrophobic pantothenate and isovalerate binding pocket (Figure 4B and C). The adenine moiety interacts with the backbone carbonyl atoms of Lys175 and Val180, residues located in a loop connecting helix α8 and α9. The phosphate groups are hydrogen-bonded to Lys175 and Lys132* (* indicating the second monomer), whereas the pantothenate part is fixed by Lys172, Trp169 and a water molecule interacting with Lys131*. The isovalerate head group points into a hydrophobic pocket that is perfectly shaped to interact with IV-CoA and is formed by Phe72*, Leu100*, Val101*, Val109*, Ile112*, Leu113*, Tyr134* and Leu168* (Figure 4C and D).

Isovaleryl coenzyme A induces an open and flexible state essential for DNA interaction

In order to track conformational changes and signal transduction upon IV-CoA and DNA binding (Figure 5A), we also determined the structure of AibR/IV-CoA in complex with a 16-bp DNA fragment of the AibR recognition sequence to 2.92 Å resolution. Different DNA constructs were used for crystallization, but only a perfect palindromic 16-bp fragment yielded well-diffracting crystals (nt 2–17 of the 18-bp inverted repeat, in which guanosine 9 has been exchanged by adenine, Figure 3A). The complex crystallized in space group I422 with two homodimers and one DNA duplex in the asymmetric unit. At first sight, two homodimers seemed to interact with two different positions of the same single double-stranded DNA molecule. However, in the course of refinement, we observed additional difference electron density for four base-pairs at one end of the double helix, indicative of the presence of a second alternative, partially shifted position of the 16-bp DNA molecule in the asymmetric unit. Therefore, we ultimately refined the structure by placing two partially occupied 16-mer DNA double

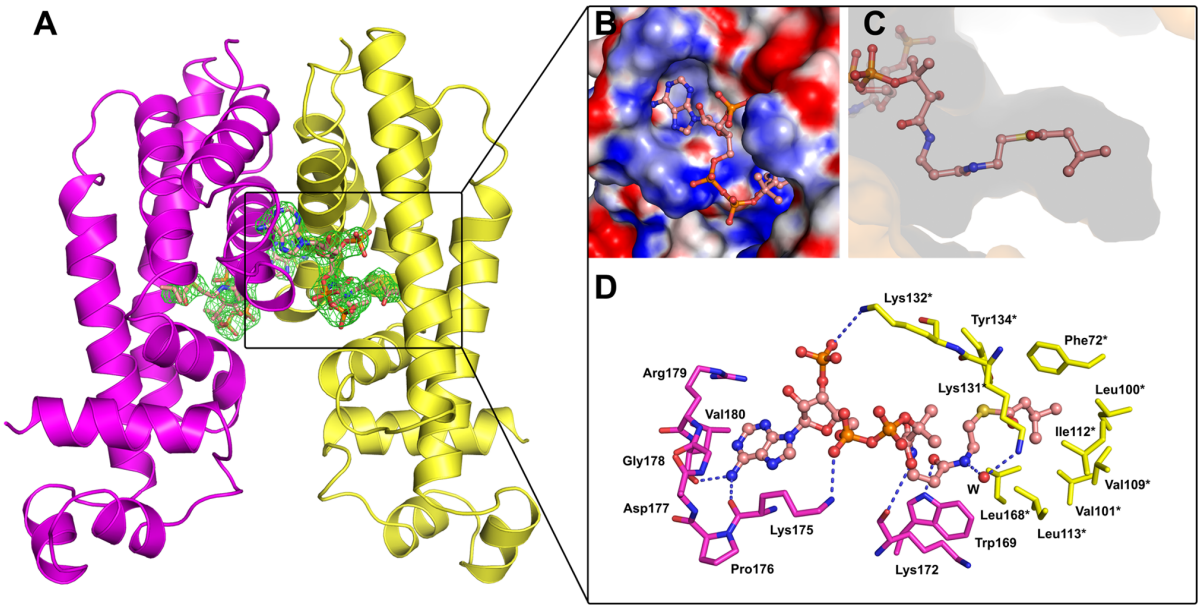

Figure 4. Structural insights into IV-CoA binding and specificity. (**A**) Overall structure of the AibR and IV-CoA complex. The difference electron density is contoured at 3σ. (**B**) Surface charge distribution of the solvent-exposed CoA binding site (calculated by using PDB2PQR (49,50)). (**C**) View into the hydrophobic IV-CoA binding pocket. (**D**) Entire interactions between AibR and IV-CoA. All molecular presentations were generated using PyMol (Schrödinger) (51).

strands as alternative conformations shifted and rotated by 4 base-pairs. With this, both AibR homodimers show the same base specific interactions, as they do not interact with only a single DNA double helix on opposite sites, but rather with two partially occupied DNA molecules contained in the protein crystal. The crystal lattice is built by protein–protein contacts only and no contacts are observed between the DNA strands, which may explain the partial occupancy of the two DNA double strands (Supplementary Figure S7).

The ligand-free form and the IV-CoA complex of AibR superimpose with an rms deviation of 1.216 Å over 4018 atoms. Interestingly, the two DNA binding domains are separated by 42.7 Å in the apo form and by 45.2 Å (between Tyr51 of each subunit) in the IV-CoA complex, which is not compatible with the gap of two consecutive DNA major grooves (Figure 5B) (16).

Major changes between the two structures involve movements of helix α1, α2, α4 and α6, mainly mediated by His114. This residue is located in the ligand-binding site and moves approx. A total of 10 Å upon IV-CoA binding to form a hydrogen bond with Tyr171 (Figure 5C). As a consequence, helix α6 elongates, leading to interruption of the hydrogen-bonding network created by Arg24, Lys107 and Glu108 and subsequently resulting in higher flexibility of α1 (Figure 5D). Additional hydrophobic repulsions and the movement of Phe72, a residue that blocks the active site in the apo from of AibR, push helix α4 outward and result in additional flexibility of α1 via the disruption of a salt bridge formed by Arg16 and Glu74 (Figure 5E).

In contrast to the IV-CoA-bound structure, the IV-CoA-DNA complex shows a condensed and rigid structure perfectly suited to interact with DNA. Helix α4 and α7 move toward the centre of AibR and α6 unfolds at the end to enable an interaction of His114 and Tyr171 of both monomers (Figure 5C). Helix α1 is stabilized in its new position through the interaction of Glu28 and Lys107 (Figure 5D). With this, Arg29 (α1) is now able to hydrogen-bond to Glu38 (α2) and stabilize the position of α2 (Figure 5F). These movements lead to a closed conformation and the reduction of the gap between the two DBDs from almost 45.2 to 36.2 Å (distance between Tyr51 of both DBDs).

Further, IV-CoA shows a slightly different binding mode in the AibR/IV-CoA/DNA complex when compared to the structure without DNA. It binds in a different conformation, but the interactions with the protein remain almost identical. The only exception is Lys131 that directly contacts the pantothenate part of IV-CoA (Figure 6A). This seems to be a consequence of the transition between the highly flexible IV-CoA and the rigid and condensed IV-CoA-DNA complex.

Together, the three structures show that IV-CoA binding renders the rigid apo form flexible, which enables proper reorientation of the DNA binding domain to interact with the operator sequence. DNA-binding then rigidifies AibR again.

Lys47 and Tyr51 are important for specific DNA sequence recognition

After DBD repositioning, helix α2 and α3 directly contact the phosphate backbone and specific bases. Both monomers show the same interactions with the DNA, hence only monomer A is discussed in this paragraph. In more detail, interactions with the DNA backbone appear between the guanidinium group of Arg14 and the phosphate group of cytosine 2, the hydroxyl group of Ser35 and the phosphate group of cytosine 11, the backbone amide of Met36 and the phosphate group of guanosine 12 and the hydroxyl group of Thr46 with the phosphate group of cytosine 2. Additional

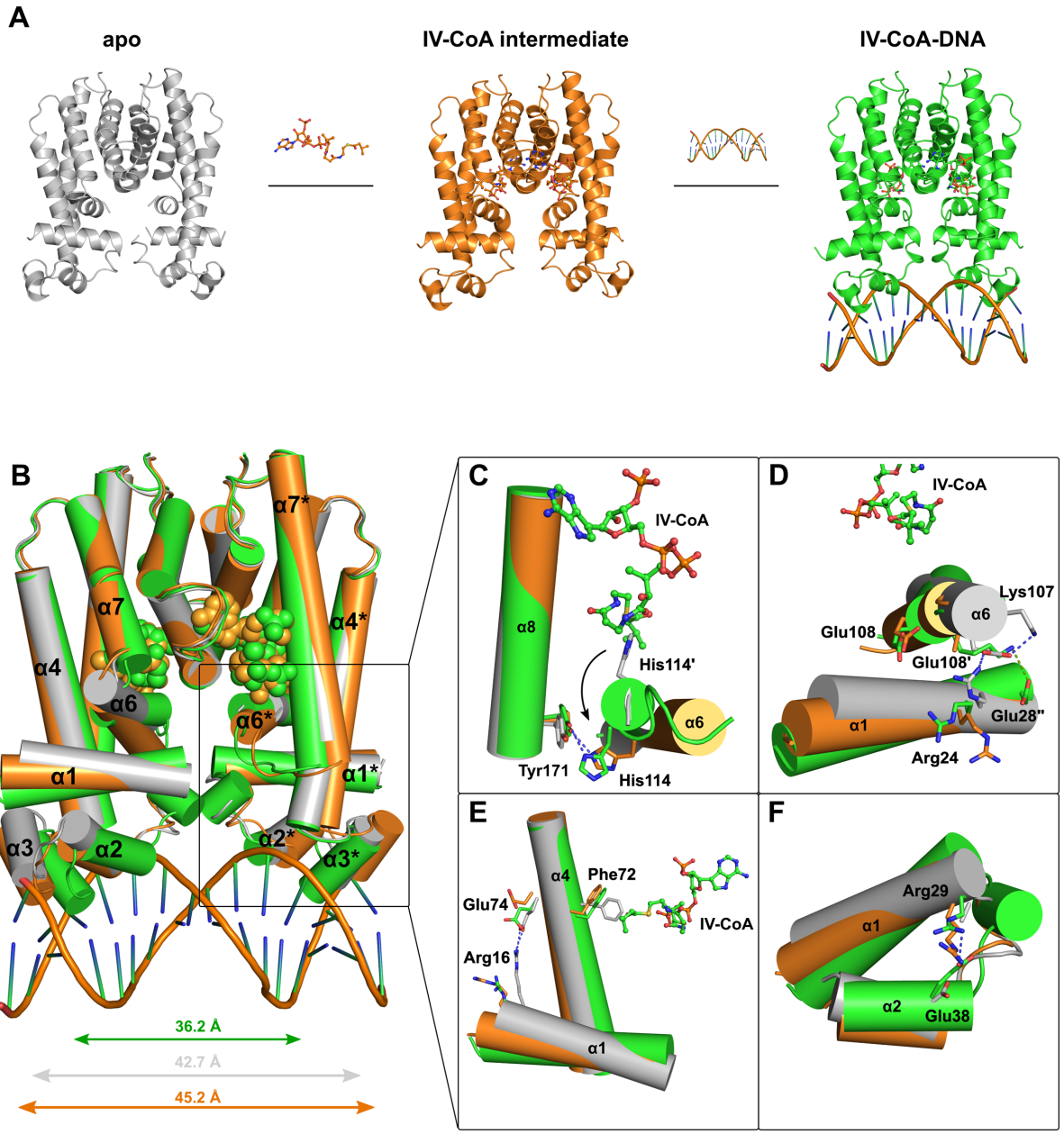

Figure 5. Comparison of apo, IV-CoA and IV-CoA and DNA bound AibR. (**A**) The apo structure (grey) represents the 'off state' of AibR where *AIB*-related genes are transcribed. IV-CoA binding results in a highly flexible intermediate (orange) that enables repositioning of the DNA binding domains to interact with the consensus sequence in the 'on state' (green). (**B**) Overall comparison of apo AibR (grey), IV-CoA (orange) and IV-CoA and DNA bound AibR (green). The distance between the DBDs was calculated using the position of Tyr51. (**C**) His114-mediated shift of α6 (' indicates apo-AibR). (**D**) Disruption of the Arg24/Lys107/Glu108-generated hydrogen-bonding network (IV-CoA and IV-CoA-DNA complex) leads to interaction of Glu28 ('indicates the IV-CoA-DNA complex) and Lys107 (IV-CoA-DNA complex) as a result of IV-CoA and DNA binding. (**E**) Disruption of the interaction between Arg16 and Glu74 upon IV-CoA binding. (**F**) Interaction between Arg29 and Glu38 in the IV-CoA-DNA complex.

hydrogen bonds with phosphate groups of the DNA are formed by the phenol moiety of Tyr51 and guanosine 13, the imidazole side chain of His53 and cytosine 2 and between the backbone amide and the ϵ-amino group of Lys57 with guanosine 12 and 13, respectively (Figure 6C and D).

In contrast, only two amino acid side chains are responsible for base-specific contacts. Here, the ϵ-amino group of Lys47 forms two hydrogen bonds to O6 of guanosine 12 and 13, whereas Tyr51 is involved in CH-π interaction with the methyl group of thymine 14. The C7 carbon atom is oriented perpendicular to the phenol moiety of Tyr51 and shows a distance of 3.7 Å, perfectly suited for such an interaction (Figure 6B and D) (39). Taken together, AibR utilizes seven amino acids in DNA backbone interactions and only two in direct base specific contacts.

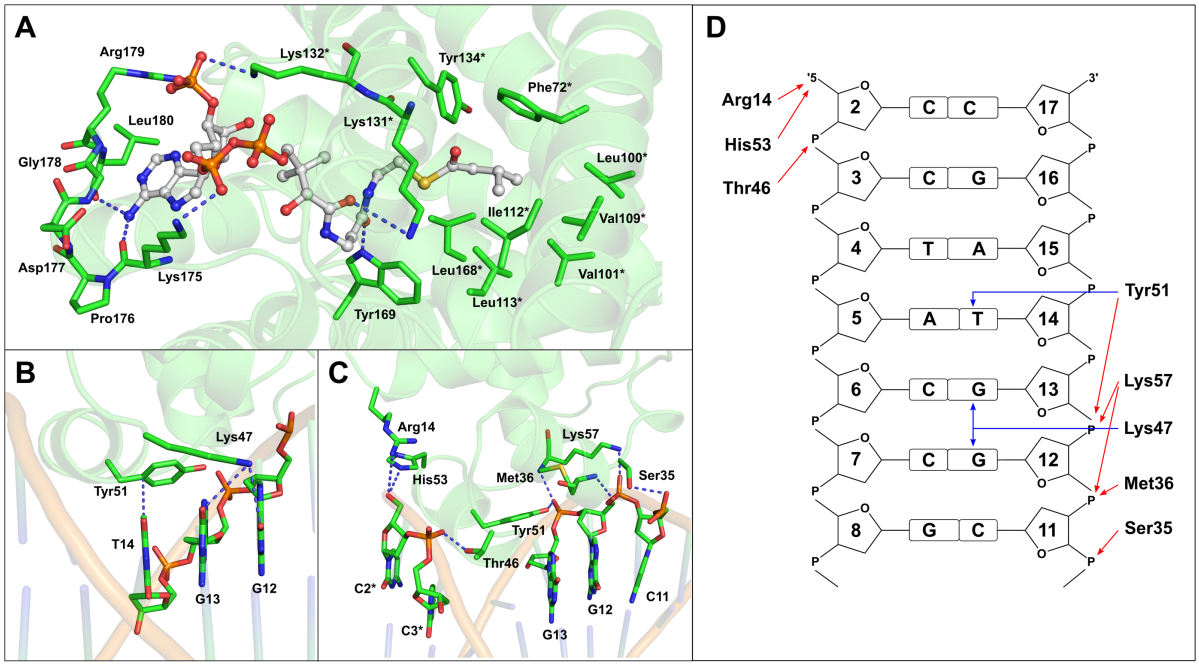

Figure 6. Interactions of AibR with IV-CoA and with the operator. (**A**) Interactions between AibR and IV-CoA (* indicates the second monomer). (**B**) Interactions of Lys47 and Tyr51 with G12, G13 and T14. (**C**) Protein–phosphate backbone interactions (* indicates the second strand). (**D**) Schematic representation of AibR-DNA interactions. Blue arrows indicate base-specific and red arrows phosphate backbone contacts. Only one half of the DNA is shown for clarity.

DISCUSSION

IV-CoA is an important metabolite in myxobacteria, since this molecule is a widely used building block in many cellular processes (3–7). This finding is mirrored in the presence of an alternative biosynthetic route that has only recently been characterized (10,11). IV-CoA generation must be properly controlled to maintain and provide sufficient levels during bacterial development. In this study, we have elucidated molecular details of the transcriptional regulation of AIB in *Myxococcus xanthus*. The system is regulated by AibR, a TetR-like transcription factor. Although the overall structure of TFRs is highly similar, the chemical identity of interaction partners, the signal transduction mechanism upon ligand binding and the specific DNA sequence recognition show significant differences within this family. We identified IV-CoA as small effector molecule of AibR and determined the K_D as 0.99 μM ± 0.35 μM. Compared to other TetR-like regulators, IV-CoA binds with unusually weak affinity. Typically, these affinities lie in the lower nanomolar range, which is a prerequisite to immediately respond to very low concentration of antibiotics or environmental changes by enabling rapid transcription of resistance machineries or other enzymes (17). Although TetR-ligands typically act agonistically, IV-CoA in the AibR/IV-CoA system functions as an antagonist that represses transcription in the effector-bound state and enables IV-CoA biogenesis in the ligand-free form, as shown by EMSA and MST analysis. This fact may explain the relatively weak binding affinity, as a certain level of IV-CoA is mandatory for the cell and thus the pathway is not shut down at low concentrations of the molecule. We identified an 18-nt near-perfect inverted repeat containing a two nucleotide spacer as the AibR binding site, in which most of the nucleotides 1–17 are important to mediate binding. Similar inverted repeats are often found in TetR-like regulatory systems and differ not only in sequence and length, but also in spacer composition. RutR (40), for example, binds to an inverted repeat separated by 5 bp, whereas HrtR or TetR interact with palindromic sequences separated by only one nucleotide (39,41).

Further, we identified an additional locus that the AibR/IV-CoA complex interacts with, although with lower affinity. This is most probably the consequence of a nucleotide exchange at position 14, a base directly involved in AibR binding (Figures 3A and 6B). In aibR8, position 14 is occupied by thymine whose methyl group is involved in CH-π interaction with Tyr51. In the novel locus, mxan_3791, the thymine is replaced by adenine such that it is no longer able to establish this interaction.

Mxan_3791 codes for a putative acetyl coenzyme A acetyltransferase (42). These enzymes catalyze the condensation of two acetyl-CoA molecules to generate acetoacetyl-CoA. Interestingly, acetoacetyl-CoA is one of the two substrates of MvaS, a 3-hydroxy-3-methylglutaryl-CoA synthase involved in the first step of AIB (Figure 1; (3,10)). Although Mxan_3791 did not appear to be up-regulated under leucine limiting conditions (10), we propose a role in AIB by providing one of the two substrates for the first enzyme of the pathway.

In order to provide detailed structural insights into effector binding, signal transmission and DNA interaction, we determined the structure of AibR in the ligand free, the IV-CoA and IV-CoA/DNA-bound form. TFR

members respond to a broad spectrum of effectors; small molecules such as uracil, more complex substances like ethidium, fatty acids or different CoA-derivatives have been identified in this regard (39,42–44). IV-CoA as the effector of AibR shows a binding mode that is similar to HIP-CoA (3aα-H-4α(3′-propanoate)-7aβ-methylhexahydro-1,5-indanedione-CoA), the ligand of *Mycobacterium tuberculosis* regulator KstR2 (45). Interestingly, the co-crystal structures of KstR, another mycobacterial regulator, in complex with 3OCh- (3-oxocholest-4-en-26-oyl-) and 4-BNC-CoA (3-oxo-23,24-bisnorchol-4-en-22-oyl-CoA) revealed different binding modes of these CoA-derivatives compared to AibR. In this protein, the CoA-binding pocket is located on the opposite site of the protein and interacts with only one monomer, again showing the diversity of TFR members (Supplementary Figure S8; (46)).

IV-CoA binding shifts His114 out of the binding site to hydrogen-bond with Tyr171. This shift induces the disruption of the hydrogen bonding networks between Arg24, Lys107 and Glu108 and Arg16 and Glu74, both connecting the LBD and the DBD in the apo form. This loss of hydrogen bonds leads to a transition of the rigid and slightly opened apo form to the highly flexible and widely opened IV-CoA-bound intermediate state. The induced flexibility is a prerequisite for proper positioning of the DNA binding domain with respect to the major groove of the cognate operator sequence. The complex with IV-CoA and DNA appeared rigid and closed again, mainly as a consequence of the direct interaction of helix α2 and α3 with the DNA backbone and with specific bases. Further, the hydrogen bonds between Glu28 and Lys107 and Arg29 and Glu38 connecting α1 with α6 and α2 provide stabilization of the operator complex. This mode of signal transduction upon effector binding is similar to TetR, characterized by a partial unfolding of helix α6 and a pendulum-like movement of helix α4. However, in contrast to IV-CoA and AibR, tetracycline binding leads to a widening of TetR, reduction in DNA affinity and consequently gene transcription (16).

Besides the different effector interactions and signal transduction mechanisms, the interaction with DNA also differs among TetR family members. TetR itself uses all residues of α3 for specific base-pair recognition, whereas CprB from *Streptomyces coelicolor* and QacR from *Staphylococcus aureus* use only four amino acids (41,47,48). Based on our complex structure of AibR/IV-CoA with DNA and EMSAs with clustered and single mutations of the 18-nt near-perfect inverted repeat, base-specific interactions are mediated between Lys47 and Tyr51 and the bases G12, G13 and T14. These bases, specifically G12, are particularly important for DNA interaction, since mutation in this region led to an almost complete loss of DNA affinity (Figure 3A and Supplementary Figure S4B). Similar contacts have been observed for HrtR, a regulator involved in heme homeostasis in lactococci (39). This TFR member uses Arg46 and Tyr50 in a pairwise interaction for specific interactions with G11 and T12. Interestingly, AibR's Tyr51 CH-π interaction with T14 is also observed for Tyr50 and T12 in HrtR. AibR is therefore the second TetR-like protein using this type of interaction.

In contrast to most other family members, the affinity of 233 ± 20 nM of the AibR/IV-CoA complex to the operator sequence is relatively low. TetR and HrtR, for example, bind their operator sequences with a K_D of 0.2 nM, indicating that tight and strong binding is important for their function. It has been stated that these strong interactions enable constant binding to the respective DNA sequences and lead to tight repression of transcription (39,41). It is therefore attractive to speculate that AibR does not block the transcription of AIB completely but rather establishes a leaky system that constantly produces small amounts of this molecule.

In this study, we were thus able to also shed light into the *in vivo* regulation of the *AIB*-operon by AibR and identified the putative acetyl-CoA acetyltransferase (mxan_3791) to potentially belong to the AibR regulon. Interestingly, AIB involves the dehydratase LiuC, which is not encoded in the *AIB*-operon. LiuC acts at a branching point between isoprenoid and alternative IV-CoA production (Figure 1). It has been shown that *liuC* is not up-regulated in leucine degradation deficient *bkd*$^-$ mutants, indicating that it is not controlled by AibR, and it has been stated that this might be important to maintain equilibrated partitioning of HMG-CoA between IV-CoA biosynthesis and mevalonate production (10,11). Therefore, since MvaS, the enzyme acting before LiuC, is part of the *AIB*-operon and under control of AibR, LiuC might not be regulated at the transcriptional level but rather by the activity of MvaS. Besides the AibR/IV-CoA system, exploring the regulatory role of LiuC might add further insight into our understanding of myxobacterial IV-CoA production.

In summary, our data suggest that the AibR/IV-CoA system controls AIB in an unusual TFR-like manner by repressing the transcription of genes located in the *AIB*-operon in the ligand-bound state (16,37). We propose that under non-starving conditions, IV-CoA is produced by leucine degradation, binds to AibR and blocks transcription of *AIB*-genes. As soon as the IV-CoA concentration drops below a certain threshold, IV-CoA diffuses from AibR. As a consequence, His114-mediated conformational rearrangements occur, leading to reduced affinity for the operator sequence and finally to *de novo* IV-CoA production.

ACCESSION NUMBERS

Diffraction data and coordinates have been deposited in the Protein Data Bank under accession code 5K7F (AibR apo), 5K7H (AibR/IV-CoA complex) and 5K7Z (AibR/IV-CoA/operator DNA complex).

SUPPLEMENTARY DATA

Supplementary Data are available at NAR Online.

ACKNOWLEDGEMENTS

The authors thank BESSYII (Helmholtz Zentrum Berlin, Germany), the Swiss Light Source (PSI, Villingen, Switzerland) and the European Synchrotron Radiation Facility (Grenoble, France) for beamline access and support and the X-ray community at Helmholtz Centre for Infection Research in Braunschweig for data collection. Dr Yanyan Li

and Dr Pavel Afonine are acknowledged for initial cloning of *aibR*, helpful discussions and for help in refinement of the AibR/IV-CoA/DNA complex. T.B. was supported by the HZI Graduate School for Infection Research.

FUNDING

Funding for open access charge: Intramural Funds.
Conflict of interest statement. None declared.

REFERENCES

1. Wenzel,S.C. and Müller,R. (2007) Myxobacterial natural product assembly lines: fascinating examples of curious biochemistry. *Nat. Prod. Rep.*, **24**, 1211–1224.
2. Gerth,K., Pradella,S., Perlova,O., Beyer,S. and Müller,R. (2003) Myxobacteria: proficient producers of novel natural products with various biological activities–past and future biotechnological aspects with the focus on the genus Sorangium. *J. Biotechnol.*, **106**, 233–253.
3. Bode,H.B., Ring,M.W., Schwär,G., Kroppenstedt,R.M., Kaiser,D. and Müller,R. (2006) 3-Hydroxy-3-Methylglutaryl-Coenzyme A (CoA) Synthase Is Involved in Biosynthesis of Isovaleryl-CoA in the Myxobacterium Myxococcus xanthus during Fruiting Body Formation. *J. Bacteriol.*, **188**, 6524–6528.
4. Downward,J. and Toal,D. (1995) Branched-chain fatty acids: the case for a novel form of cell-cell signalling during Myxococcus xanthus development. *Mol. Microbiol.*, **16**, 171–175.
5. Hoiczyk,E., Ring,M.W., McHugh,C.A., Schwär,G., Bode,E., Krug,D., Altmeyer,M.O., Lu,J.Z. and Bode,H.B. (2009) Lipid body formation plays a central role in cell fate determination during developmental differentiation of Myxococcus xanthus. *Mol. Microbiol.*, **74**, 497–517.
6. Ring,M.W., Schwär,G., Thiel,V., Dickschat,J.S., Kroppenstedt,R.M., Schulz,S. and Bode,H.B. (2006) Novel iso-branched ether lipids as specific markers of developmental sporulation in the myxobacterium myxococcus xanthus. *J. Biol. Chem.*, **281**, 36691–36700.
7. Toal,D.R., Clifton,S.W., Roe,B.A. and Downard,J. (1995) The esg locus of Myxococcus xanthus encodes the E1α and E1β subunits of a branched-chain keto acid dehydrogenase. *Mol. Microbiol.*, **16**, 177–189.
8. Hoiczyk,E., Ring,M.W., McHugh,C.A., Schwär,G., Bode,E., Krug,D., Altmeyer,M.O., Lu,J.Z. and Bode,H.B. (2009) Lipid body formation plays a central role in cell fate determination during developmental differentiation of Myxococcus xanthus. *Mol. Microbiol.*, **74**, 497–517.
9. Downward,J. and Toal,D. (1995) Branched-chain fatty acids: the case for a novel form of cell-cell signalling during Myxococcus xanthus development. *Mol. Microbiol.*, **16**, 171–175.
10. Bode,H.B., Ring,M.W., Schwär,G., Altmeyer,M.O., Kegler,C., Jose,I.R., Singer,M. and Müller,R. (2009) Identification of additional players in the alternative biosynthesis pathway to isovaleryl-CoA in the myxobacterium Myxococcus xanthus. *Chembiochem*, **10**, 128–140.
11. Li,Y., Luxenburger,E. and Müller,R. (2013) An alternative isovaleryl CoA biosynthetic pathway involving a previously unknown 3-methylglutaconyl CoA decarboxylase. *Angew. Chem. Int. Ed Engl.*, **52**, 1304–1308.
12. Bock,T., Kasten,J., Müller,R. and Blankenfeldt,W. (2016) Crystal structure of the HMG-CoA synthase MvaS from the gram-negative bacterium Myxococcus xanthus. *Chembiochem*, **17**, 1257–1262.
13. Hao,T., Biran,D., Velicer,G.J. and Kroos,L. (2002) Identification of the Omega4514 regulatory region, a developmental promoter of Myxococcus xanthus that is transcribed in vitro by the major vegetative RNA polymerase. *J. Bacteriol.*, **184**, 3348–3359.
14. Hillen,W., Klock,G., Kaffenberger,I., Wray,L.V. and Reznikoff,W.S. (1982) Purification of the TET repressor and TET operator from the transposon Tn10 and characterization of their interaction. *J. Biol. Chem.*, **257**, 6605–6613.
15. Ramos,J.L., Martínez-Bueno,M., Molina-Henares,A.J., Terán,W., Watanabe,K., Zhang,X., Gallegos,M.T., Brennan,R. and Tobes,R. (2005) The TetR family of transcriptional repressors. *Microbiol. Mol. Biol. Rev.*, **69**, 326–356.
16. Yu,Z., Reichheld,S.E., Savchenko,A., Parkinson,J. and Davidson,A.R. (2010) A comprehensive analysis of structural and sequence conservation in the TetR family transcriptional regulators. *J. Mol. Biol.*, **400**, 847–864.
17. Cuthbertson,L. and Nodwell,J.R. (2013) The TetR family of regulators. *Microbiol. Mol. Biol. Rev.*, **77**, 440–475.
18. Feng,Y. and Cronan,J.E. (2011) Complex binding of the FabR repressor of bacterial unsaturated fatty acid biosynthesis to its cognate promoters: Complex binding of FabR repressor. *Mol. Microbiol.*, **80**, 195–218.
19. van Aalten,D.M.F. (2001) The structural basis of acyl coenzyme A-dependent regulation of the transcription factor FadR. *EMBO J.*, **20**, 2041–2050.
20. Arabolaza,A., D'Angelo,M., Comba,S. and Gramajo,H. (2010) FasR, a novel class of transcriptional regulator, governs the activation of fatty acid biosynthesis genes in Streptomyces coelicolor: Transcriptional regulation of fatty acid biosynthesis in S. coelicolor. *Mol. Microbiol.*, **78**, 47–63.
21. Irzik,K., van Ooyen,J., Gätgens,J., Krumbach,K., Bott,M. and Eggeling,L. (2014) Acyl-CoA sensing by FasR to adjust fatty acid synthesis in Corynebacterium glutamicum. *J. Biotechnol.*, **192**, 96–101.
22. Fw,S. (2013) Stable expression clones and auto-induction for protein production in E. coli. *Methods Mol. Biol.*, **1091**, 17–32.
23. Wienken,C.J., Baaske,P., Rothbauer,U., Braun,D. and Duhr,S. (2010) Protein-binding assays in biological liquids using microscale thermophoresis. *Nat. Commun.*, **1**, 100.
24. Volz,C., Kegler,C. and Müller,R. (2012) Enhancer binding proteins act as hetero-oligomers and link secondary metabolite production to myxococcal development, motility, and predation. *Chem. Biol.*, **19**, 1447–1459.
25. Schneider,C.A., Rasband,W.S. and Eliceiri,K.W. (2012) NIH Image to ImageJ: 25 years of image analysis. *Nat. Methods*, **9**, 671–675.
26. Brown,A.M. (2001) A step-by-step guide to non-linear regression analysis of experimental data using a Microsoft Excel spreadsheet. *Comput. Methods Programs Biomed.*, **65**, 191–200.
27. Kemmer,G. and Keller,S. (2010) Nonlinear least-squares data fitting in Excel spreadsheets. *Nat. Protoc.*, **5**, 267–281.
28. Shaw Stewart,P.D., Kolek,S.A., Briggs,R.A., Chayen,N.E. and Baldock,P.F.M. (2011) Random microseeding: a theoretical and practical exploration of seed stability and seeding techniques for successful protein crystallization. *Cryst. Growth Des.*, **11**, 3432–3441.
29. Mueller,U., Förster,R., Hellmig,M., Huschmann,F.U., Kastner,A., Malecki,P., Pühringer,S., Röwer,M., Sparta,K., Steffien,M. *et al.* (2015) The macromolecular crystallography beamlines at BESSY II of the Helmholtz-Zentrum Berlin: current status and perspectives. *Eur. Phys. J. Plus*, **130**, 141–150
30. Kabsch,W. (2010) Xds. *Acta Crystallogr. Sect. Biol. Crystallogr.*, **66**, 125–132.
31. Krug,M., Weiss,M.S., Heinemann,U. and Mueller,U. (2012) XDSAPP: a graphical user interface for the convenient processing of diffraction data using XDS. *J. Appl. Crystallogr.*, **45**, 568–572.
32. Winn,M.D., Ballard,C.C., Cowtan,K.D., Dodson,E.J., Emsley,P., Evans,P.R., Keegan,R.M., Krissinel,E.B., Leslie,A.G.W., McCoy,A. *et al.* (2011) Overview of the CCP4 suite and current developments. *Acta Crystallogr. Sect. Biol. Crystallogr.*, **67**, 235–242.
33. Pape,T. and Schneider,T.R. (2004) HKL2MAP: a graphical user interface for macromolecular phasing with SHELX programs. *J. Appl. Crystallogr.*, **37**, 843–844.
34. Adams,P.D., Afonine,P.V., Bunkoczi,G., Chen,V.B., Davis,I.W., Echols,N., Headd,J.J., Hung,L.-W., Kapral,G.J., Grosse-Kunstleve,R.W. *et al.* (2010) PHENIX: a comprehensive Python-based system for macromolecular structure solution. *Acta Crystallogr. Sect. Biol. Crystallogr.*, **66**, 213–221.
35. Emsley,P., Lohkamp,B., Scott,W.G. and Cowtan,K. (2010) Features and development of Coot. *Acta Crystallogr. Sect. Biol. Crystallogr.*, **66**, 486–501.
36. Schomaker,V. and Trueblood,K.N. (1968) On the rigid-body motion of molecules in crystals. *Acta Crystallogr. B*, **24**, 63–76.
37. Moriarty,N.W., Grosse-Kunstleve,R.W. and Adams,P.D. (2009) electronic Ligand Builder and Optimization Workbench (eLBOW): a tool for ligand coordinate and restraint generation. *Acta Crystallogr. D Biol. Crystallogr.*, **65**, 1074–1080.

38. Chen,V.B., Arendall,W.B., Headd,J.J., Keedy,D.A., Immormino,R.M., Kapral,G.J., Murray,L.W., Richardson,J.S. and Richardson,D.C. (2010) MolProbity: all-atom structure validation for macromolecular crystallography. *Acta Crystallogr. Sect. Biol. Crystallogr.*, **66**, 12–21.
39. Sawai,H., Yamanaka,M., Sugimoto,H., Shiro,Y. and Aono,S. (2012) Structural basis for the transcriptional regulation of heme homeostasis in Lactococcus lactis. *J. Biol. Chem.*, **287**, 30755–30768.
40. Nguyen Le Minh,P., de Cima,S., Bervoets,I., Maes,D., Rubio,V. and Charlier,D. (2015) Ligand binding specificity of RutR, a member of the TetR family of transcription regulators in Escherichia coli. *FEBS Open Bio.*, **5**, 76–84.
41. Orth,P., Schnappinger,D., Hillen,W., Saenger,W. and Hinrichs,W. (2000) Structural basis of gene regulation by the tetracycline inducible Tet repressor-operator system. *Nat. Struct. Biol.*, **7**, 215–219.
42. Goldman,B.S., Nierman,W.C., Kaiser,D., Slater,S.C., Durkin,A.S., Eisen,J.A., Eisen,J., Ronning,C.M., Barbazuk,W.B., Blanchard,M. *et al.* (2006) Evolution of sensory complexity recorded in a myxobacterial genome. *Proc. Natl. Acad. Sci. U.S.A.*, **103**, 15200–15205.
43. Itou,H., Watanabe,N., Yao,M., Shirakihara,Y. and Tanaka,I. (2010) Crystal structures of the multidrug binding repressor Corynebacterium glutamicum CgmR in complex with inducers and with an operator. *J. Mol. Biol.*, **403**, 174–184.
44. Miller,D.J., Zhang,Y.-M., Subramanian,C., Rock,C.O. and White,S.W. (2010) Structural basis for the transcriptional regulation of membrane lipid homeostasis. *Nat. Struct. Mol. Biol.*, **17**, 971–975.
45. Crowe,A.M., Stogios,P.J., Casabon,I., Evdokimova,E., Savchenko,A. and Eltis,L.D. (2015) Structural and functional characterization of a ketosteroid transcriptional regulator of Mycobacterium tuberculosis. *J. Biol. Chem.*, **290**, 872–882.
46. Ho,N.A.T., Dawes,S.S., Crowe,A.M., Casabon,I., Gao,C., Kendall,S.L., Baker,E.N., Eltis,L.D. and Lott,J.S. (2016) The structure of the transcriptional repressor KstR in complex with CoA thioester cholesterol metabolites sheds light on the regulation of cholesterol catabolism in mycobacterium tuberculosis. *J. Biol. Chem.*, **291**, 7256–7266.
47. Bhukya,H., Bhujbalrao,R., Bitra,A. and Anand,R. (2014) Structural and functional basis of transcriptional regulation by TetR family protein CprB from S. coelicolor A3(2). *Nucleic Acids Res.*, **42**, 10122–10133.
48. Schumacher,M.A., Miller,M.C., Grkovic,S., Brown,M.H., Skurray,R.A. and Brennan,R.G. (2002) Structural basis for cooperative DNA binding by two dimers of the multidrug-binding protein QacR. *EMBO J.*, **21**, 1210–1218.
49. Dolinsky,T.J., Czodrowski,P., Li,H., Nielsen,J.E., Jensen,J.H., Klebe,G. and Baker,N.A. (2007) PDB2PQR: expanding and upgrading automated preparation of biomolecular structures for molecular simulations. *Nucleic Acids Res.*, **35**, W522–W525.
50. Dolinsky,T.J., Nielsen,J.E., McCammon,J.A. and Baker,N.A. (2004) PDB2PQR: an automated pipeline for the setup of Poisson–Boltzmann electrostatics calculations. *Nucleic Acids Res.*, **32**, W665–W667.
51. The PyMOL Molecular Graphics System, Version 1.7.4 Schrödinger, LLC, https://www.pymol.org/citing.